A Model for the Interaction between 2-Day Waves and Moist Kelvin Waves*

FEI LIU

International Pacific Research Center, University of Hawaii at Manoa, Honolulu, Hawaii

BIN WANG

International Pacific Research Center, and Department of Meteorology, University of Hawaii at Manoa, Honolulu, Hawaii

(Manuscript received 26 April 2011, in final form 16 August 2011)

ABSTRACT

The eastward-propagating tropical low-frequency disturbances, such as the moist Kelvin waves or the Madden–Julian oscillation (MJO), are often observed to experience convective enhancement when meeting with the westward-propagating 2-day waves. A scale interaction (SI) model is built to understand the nature of the interaction between the 2-day waves and moist Kelvin waves or MJO. In this model, the convective complex of moist Kelvin waves modulates the strength and location of the 2-day waves, which feed back through the upscale eddy transfer. An ageostrophic model describing the 2-day waves is first solved, and the resultant westward-propagating, backward-tilted disturbances are consistent with the observed 2-day waves. An explicit representation of eddy momentum transfer (EMT), eddy heating transfer (EHT), and eddy moisture transfer (EQT) arising from the 2-day waves is then formulated. The SI model shows that the 2-day waves in front of moist Kelvin waves produce an EMT accelerating the low-frequency easterly in the lower troposphere, an EHT cooling down the middle troposphere, and an EQT moistening the middle troposphere. These three transfer terms have comparable magnitude. Although the negative EHT tends to damp the moist Kelvin waves, both the EMT and EQT provide instability sources for the moist Kelvin waves. The 2-day waves also slow down the moist Kelvin waves, mainly through the advective effects of the EMT. So the unstable moist Kelvin waves may exhibit convective enhancement when meeting with the 2-day waves. The theoretical results presented here point to the need to further observe the multiscale structures within the moist Kelvin waves and the MJO.

1. Introduction

Recent observations have revealed that the Madden–Julian oscillation (MJO) (Madden and Julian 1971, 1994) may involve scale interaction (SI) among the MJO, moist Kelvin waves, and 2-day waves (Nakazawa 1988; Kikuchi and Wang 2010, hereafter KW10). Using the spatial–temporal (two-dimensional) wavelet transform to detect nonstationary wave propagation signals from a time–space domain of the outgoing longwave radiation (OLR), KW10 found that 1) the 2-day waves are more active to the east of the low-frequency moist active convective area, especially for the MJO (Fig. 1), and 2) the low-frequency, eastward-propagating moist Kelvin waves and MJO exhibit convective enhancement when meeting the westward-propagating 2-day waves (Figs. 1 and 2). But it remains elusive why such convective enhancement occurs.

In an SI system, the convective momentum transfer is a process that can convert convective available potential energy (CAPE) to large-scale horizontal kinetic energy, which can change from the downscale to upscale in the westerly burst regime of the MJO (Tung and Yanai 2002a,b). Moncrieff (2004) proposed that the upscale momentum and heat transfers may play an important role in maintaining the MJO. Majda and Biello (2004) obtained an eddy momentum transfer (EMT) parameterization for

* School of Ocean and Earth Science and Technology Contribution Number 8505 and International Pacific Research Center Publication Number 820.

Corresponding author address: Dr. Bin Wang, IPRC and Department of Meteorology, University of Hawaii at Manoa, 401 POST Bldg., 1680 East-West Road, Honolulu, HI 96822.
E-mail: wangbin@hawaii.edu

DOI: 10.1175/JAS-D-11-0116.1

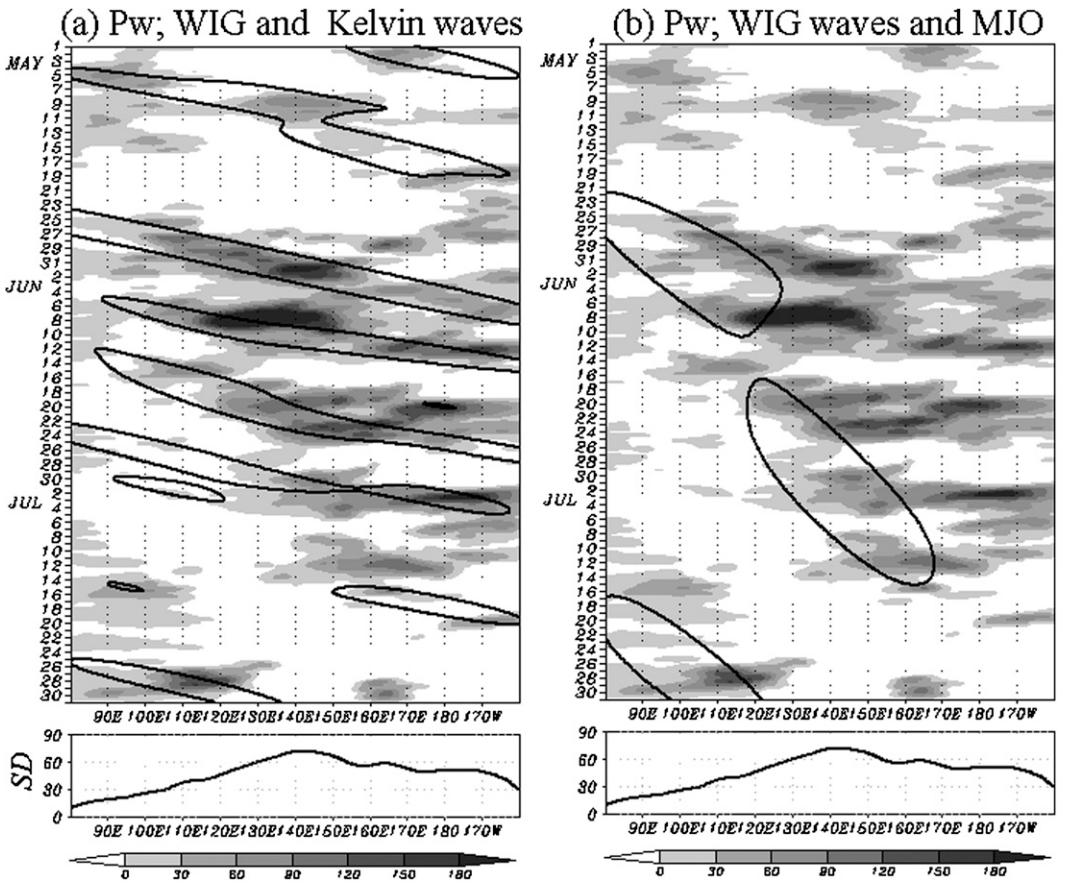

FIG. 1. Hovmöller diagram of local wavelet scalogram anomaly (K^2) that corresponds to the westward inertio-gravity (WIG) wave component. The anomaly is defined as the deviation from the May–July mean at each point and linear trend is also removed. Positive (negative) values are shaded (contoured). Thick solid lines indicate contour lines at −5 K of infrared data for (a) the Kelvin wave and (b) the MJO component (adapted from KW10).

the eastward-propagating super cloud clusters (SCCs) and simulated the MJO structure from the EMT of SCCs. The same but out-of-phase EMT parameterization was also used for describing the westward-propagating 2-day waves by Biello and Majda (2005). They pointed out that both the SCCs and 2-day waves can affect the MJO through the upscale EMT. However, the geostrophic approximation was used when deriving the solution of SCCs and 2-day waves (Majda and Biello 2004; Biello and Majda 2005). Compared with the EMT, the resulting eddy heating transfer (EHT) was negligibly small.

Rigorously speaking, the geostrophic approximation is not valid for the equatorial 2-day waves (Takayabu 1994), which are identified as $n = 1$ westward inertio-gravity waves with wavelength of about 2500 km and period of about 2 days by Takayabu et al. (1996) and Haertel and Kiladis (2004) using observations, and by Haertel and Kiladis (2004) and Haertel et al. (2008) using numerical simulations. A correct solution for the 2-day waves is a prerequisite for an adequate parameterization of their upscale transfer of eddy momentum, heat, and moisture and for understanding their roles in the moist Kelvin waves.

The MJO and moist Kelvin waves have a so-called ''self-similarity'' cloud structure: The deep convection is led by congestus clouds and tailed by stratiform clouds (Mapes et al. 2006; Kiladis et al. 2009). The congestus clouds precondition the moisture for the development of deep convection (Maloney and Hartmann 1998; Johnson et al. 1999). The 2-day waves are also active to the east of the major deep convection center (KW10). Observations reveal that the 2-day waves experience strong moisture perturbations, especially in the lower troposphere (Takayabu et al. 1996; Haertel and Kiladis 2004). Therefore, we hypothesize that the eddy moisture transfer (EQT) associated with the 2-day waves may also be important for understanding the SI between the 2-day waves and MJO or moist Kelvin waves.

The MJO is an equatorial planetary-scale circulation system that moves eastward slowly (~5 m s^{-1}), and it has

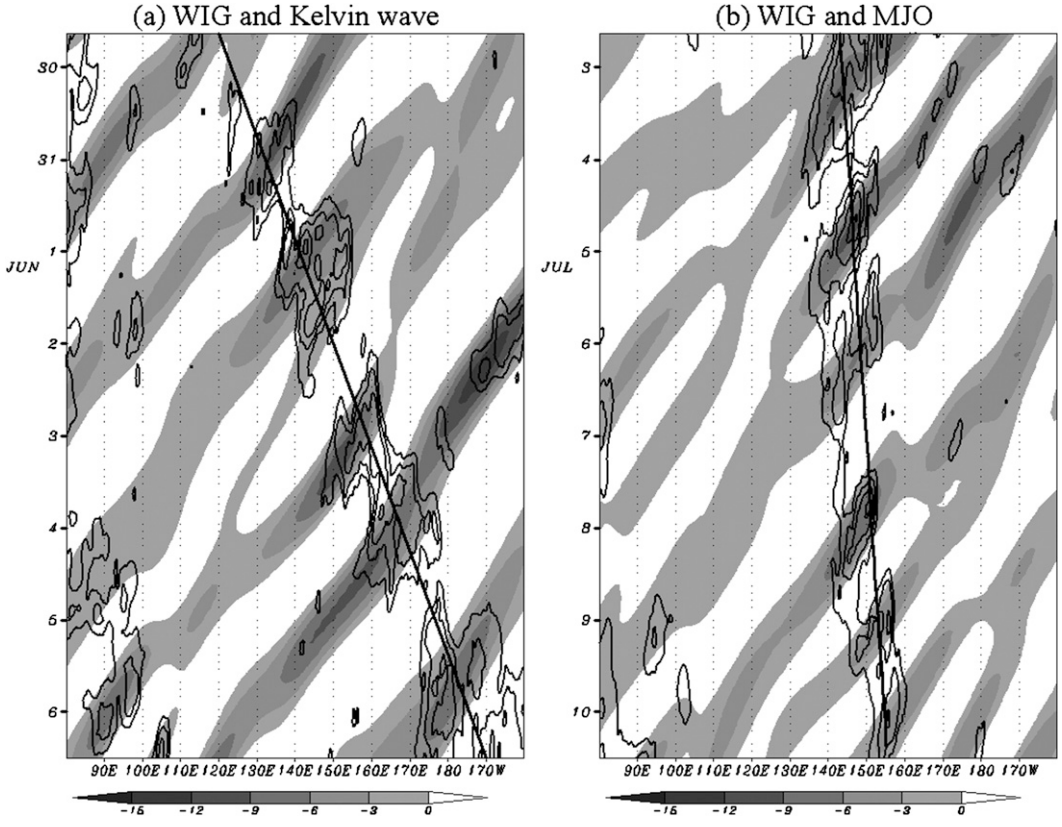

FIG. 2. Hovmöller diagram of lower-frequency component (1–2.5-day period) of WIG waves (shading) within (a) a Kelvin wave averaged between 0° and 10°N and (b) the MJO averaged between 5°S and 5°N. Low infrared values (<250 W m^{-2}) of nonfiltered data are superposed as contour lines with an interval of 10 W m^{-2} (adapted from KW10).

a prominent Kelvin wave component with wavenumbers 1 and 2 (Wang and Rui 1990). The moist Kelvin waves are more active at wavenumbers 3–6 (Wheeler and Kiladis 1999). In this paper we focus on the interaction between the high-frequency 2-day waves and the low-frequency moist Kelvin waves with wavenumbers 1 (~40 000 km)–8 (~5000 km). The understanding gained from this SI model is also helpful to understand the interaction between the 2-day waves and the MJO.

Based on the aforementioned physical consideration, we propose a prototype model in section 2 for studying the interaction between the 2-day waves and moist Kelvin waves. The model is built to include two essential physical processes. First, the convective complex of the low-frequency moist Kelvin waves modulates the strength and location of the high-frequency 2-day waves; and second, the 2-day waves feed back to the moist Kelvin waves through the upscale eddy momentum, heat, and moisture transfers. To build such a SI model, a correct solution of the 2-day waves must be derived first (section 3). Based on this solution we can then obtain an explicit representation of the EMT, EHT, and EQT (section 4). Finally, we will parameterize the eddy flux envelope and investigate the role of 2-day waves in the moist Kelvin dynamics (section 5). The result is relevant to understanding the convective enhancement of moist Kelvin waves.

2. The model

The theoretical model used here is based on the intraseasonal, planetary equatorial synoptic dynamics (IPESD) model derived by Majda and Klein (2003), which are the constant-buoyancy-frequency Boussinesq equations with a standard troposphere value for the buoyancy frequency. We implemented a moisture equation to discuss the moist dynamics. The rigid-lid boundary conditions, with no vertical flow at the bottom (900 hPa) and top (100 hPa) of the free troposphere, are used, following the works of Majda and Biello (2004) and Biello and Majda (2005). These vertical boundary conditions are reasonable approximations for capturing the middle and lower tropospheric dynamics of the 2-day waves (Haertel and Kiladis 2004). Below u, v, and ω denote the x, y, and p (zonal,

meridional, and vertical pressure) components of velocity, respectively, where x and y represent horizontal distances, p is the pressure, and t is the time. The remaining dynamic variables are the disturbed geopotential ϕ, temperature T, moisture (mixing ratio) q, and the diabatic heating Q.

The primitive equations are written on the β plane:

$$u_t - \beta y v + \phi_x = 0, \tag{1}$$

$$v_t + \beta y u + \phi_y = 0, \tag{2}$$

$$u_x + v_y + \omega_p = 0, \tag{3}$$

$$\phi_p = -\frac{R}{p}T, \tag{4}$$

$$T_t - \frac{p}{R}S\omega = Q, \tag{5}$$

$$q_t + \tilde{M}\omega = -\frac{C_p}{bL_q}Q, \tag{6}$$

where $R = 287$ J kg^{-1} K^{-1} is the specific gas constant, $C_p = 1004$ J kg^{-1} K^{-1} is the specific heat at constant pressure, $L_q = 2.5 \times 10^6$ J kg^{-1} is the latent heat of condensation, and $S = (T/\theta)\partial\theta/\partial P$ is the static stability parameter. Also, b is fractional moisture converted into rainfall (Wang 1988; here we take $b = 0.5$) and $\tilde{M}$ is the background mean moisture gradient (as for the temperature in the Boussinesq equations), which is obtained from a mean sounding (Frierson et al. 2004). Observations show that the eastward-propagating moist Kelvin waves have a typical wavelength of about 10 000 km and a period of above 10 days, while the westward-propagating 2-day waves have a typical wavelength of about 2500 km and a period of about 2 days. As such, the moist Kelvin waves can be seen as an envelope of equatorial 2-day waves. The zonal and temporal variables are (X, t_L) and (x, t) for the low- and high-frequency motions, respectively; $(X, t_L) = \varepsilon(x, t)$, where ε is the Froude number (Majda and Klein 2003). The variables of the flow can be separated into means and fluctuations on the 2-day wave scale. A given atmospheric variable $G(X, x, y, p, t)$ can be expressed as

$$G(X, x, y, p, t) = \overline{G}(X, y, p, t_L) + g(X, x, y, p, t), \tag{7}$$

where

$$\overline{G}(X, y, p, t_L) = \frac{1}{4L_0T_0}\int_{-T_0}^{T_0}\int_{-L_0}^{L_0} g(X, x, y, p, t)\,dx\,dt. \tag{8}$$

Here we introduce the characteristic values: $p_H = p_0/\pi$, $C = \sqrt{p_H^2 S}$, $(x, y) = (x', y')\sqrt{C\beta^{-1}}$, $X = X'\varepsilon^{-1}\sqrt{C\beta^{-1}}$, $p - 100$ hPa $= p' p_H$, $t = t'/\sqrt{C\beta}$, $t_L = t'_L\varepsilon^{-1}/\sqrt{C\beta}$, $(u, v, \overline{U}) = (u', v', \overline{U}')\varepsilon C$, $\omega = \omega'\varepsilon p_H\sqrt{C\beta}$, $\overline{\Omega} = \overline{\Omega}'\varepsilon^2 p_H\sqrt{C\beta}$, $(\phi, \overline{\Phi}) = (\phi', \overline{\Phi}')\varepsilon C^2$, $(T, \overline{T}) = (T', \overline{T}')\varepsilon p_M C^2/(Rp_H)$, $(q, \overline{q}) = (q', \overline{q}')\varepsilon p_M C_p C^2/(Rp_H L_q)$, $Q = Q'\varepsilon p_M C^2\sqrt{C\beta}/(Rp_H)$, and $\overline{Q} = \overline{Q}'\varepsilon^2 p_M C^2\sqrt{C\beta}/(Rp_H)$. Note that p_0 is the free tropospheric depth, and p_M is the middle tropospheric height. By this definition p' decreases upward from π to 0. Hereafter the primes in the nondimensional equations will be omitted for simplicity.

Without the effect of the moist Kelvin waves, the nondimensional equations for the 2-day waves can be written as

$$u_t - yv + \phi_x = 0, \tag{9}$$

$$v_t + yu + \phi_y = 0, \tag{10}$$

$$u_x + v_y + \omega_p = 0, \tag{11}$$

$$\phi_p = -T, \tag{12}$$

$$T_t - \omega = Q, \tag{13}$$

$$q_t + \tilde{M}\omega = -Q. \tag{14}$$

The nondimensional SI model for the moist Kelvin waves can be written as

$$\overline{U}_{t_L} = -\overline{\Phi}_X + F^U, \tag{15}$$

$$y\overline{U} = -\overline{\Phi}_y, \tag{16}$$

$$\overline{U}_X + \overline{\Omega}_p = 0, \tag{17}$$

$$\overline{T} = -\overline{\Phi}_p, \tag{18}$$

$$\overline{T}_{t_L} - \overline{\Omega} = \overline{Q} + F^T, \tag{19}$$

$$\overline{q}_{t_L} + \overline{\tilde{M}}\overline{\Omega} = -\overline{Q} + F^q, \tag{20}$$

where the three eddy forcing terms, F^U, F^T, and F^q, are the EMT, EHT, and, EQT, respectively. The scale parameters of the model are listed in Table 1.

3. The solution of 2-day waves

Based on the observed structures (Takayabu et al. 1996; Haertel and Kiladis 2004), the 2-day waves can be represented by the first two baroclinic modes. So the dependent variables can be separated into

$$\{u, v, \phi\} = -\sum_{j=1,2}\{u_j, v_j, \phi_j\}\cos(jp) \quad \text{and} \tag{21a}$$

TABLE 1. List of scale parameters of the model.

Physical quantity	Name	Value
Equatorial β parameter	$\beta = f_y$	2.3×10^{-11} m^{-1} s^{-1}
Free tropospheric depth	p_0	800 hPa
Middle tropospheric height	p_M	500 hPa
Mean static stability	S	3×10^{-6} m^2 s^{-2} Pa^{-2}
Mean vertical moisture gradient	$\tilde{Q}, \overline{\tilde{Q}}$	~0.9
Froude number	ε	0.2
Vertical scale	p_H	p_0/π, 254.6 hPa
Reference wave speed	C	$\sqrt{Sp_H^2}$, 44 m s^{-1}
Meridional scale	y	$\sqrt{C\beta^{-1}}$, 1385 km
Synoptic zonal scale	x	$\sqrt{C\beta^{-1}}$, 1385 km
Planetary zonal scale	X	$\varepsilon^{-1}\sqrt{C\beta^{-1}}$, 6924 km
Synoptic time scale	t	$1/\sqrt{C\beta}$, 0.36 day
Planetary time scale	t_L	$\varepsilon^{-1}/\sqrt{C\beta}$, 1.8 days
Horizontal velocity scale	$u, v, \overline{U}$	εC, 8.8 m s^{-1}
Synoptic vertical pressure velocity scale	ω	$\varepsilon p_H\sqrt{C\beta}$, 0.16 hPa s^{-1}
Planetary vertical pressure velocity scale	$\overline{\Omega}$	$\varepsilon^2 p_H\sqrt{C\beta}$, 0.03 hPa s^{-1}
Temperature scale	$T, \overline{T}$	$\varepsilon p_M C^2/Rp_H$, 2.6 K
Moisture scale	$q, \overline{q}$	TC_p/bL_q, 2.2 g kg^{-1}
Geopotential scale	$\phi, \overline{\Phi}$	εC^2, 389 m^2 s^{-1}
Synoptic heating scale	Q	$\varepsilon p_M C^2\sqrt{C\beta}/Rp_H$, 7.3 K day^{-1}
Planetary heating scale	$\overline{Q}$	$\varepsilon^2 p_M C^2\sqrt{C\beta}/Rp_H$, 1.5 K day^{-1}

$$\{T, \omega, q\} = \sum_{j=1,2} \{T_j, \omega_j, q_j\} \sin(jp), \qquad (21b)$$

where $j = 1$ and 2, denote the first and second baroclinic modes, respectively.

Observations show that the 2-day waves exhibit eastward tilt with height against their westward propagation, where the congestus clouds lead (in the direction of westward propagation) the deep convection, and the stratiform clouds follow the deep convection (Takayabu et al. 1996; Haertel and Kiladis 2004; Haertel et al. 2008). Usually, the latent heat released in the deep convection warms up the entire tropospheric column with a maximum in the middle troposphere. The congestus clouds warm up the lower troposphere but cool down the upper troposphere. In contrast, the stratiform clouds warm up the upper troposphere and cool down the lower troposphere (Mapes 2000; Khouider and Majda 2006, 2007; Waite and Khouider 2009). So the diabatic heating is composed of deep convective ($j = 1$), congestus ($j = 2_+$), and stratiform heating ($j = 2_-$). Here we specify the phase relationship between the two baroclinic modes, namely 1) a positive second baroclinic mode ($j = 2_+$) associated with congestus clouds (bottom-heavy heating profile), which leads (in the direction of westward propagation) to the first baroclinic mode ($j = 1$) associated with deep convection by a phase ϕ_0; and 2) a negative second baroclinic mode ($j = 2_-$) associated with stratiform clouds (top-heavy heating profile), which tails the first baroclinic mode by the same phase ϕ_0. That leads to

$$Q = F(X) \sum_{j=1,2+,2-} Q_j \cos(kx + \phi_j) \sin(jp), \quad (22)$$

where $\phi_1 = 0$, and $\phi_{2+} = -\phi_{2-} = \phi_0$, which means that in the propagating direction of 2-day waves, the congestus heating leads the deep convective heating, and the stratiform heating follows the deep convective heating by the same phase ϕ_0. We have assumed that for the 2-day waves, the stratiform and congestus heating are equal, and each one occupies one-third of the deep convective heating (i.e., $Q_{2+} = -Q_{2-} = Q_1/3$). The envelope of 2-day waves is $F(X) = \cos[\pi(X - 180°)/2L_x]$ when $|X - 180°| \le L_x$, and $F(X) = 0$ when $|X - 180°| > L_x$. This envelope spans 60° with center at 180° when $L_x = 30°$.

The diabatic heating Q_j can be represented by

$$Q_j = -H_j\omega_j, \qquad (23)$$

where H_j is an arbitrary positive constant. This is based on a conception that has observational support for the 2-day waves (Haertel and Kiladis 2004; Haertel et al. 2008). The negative heating is a simplification for dealing with the anomalous heating, and it represents a suppressed phase of 2-day waves similar to that shown in observations (Haertel and Kiladis 2004).

The standard nondimensional $\tilde{M}$ is close to 0.9 (Yano and Emanuel 1991; Frierson et al. 2004), which is similar to the intensity of the interior wave convergence-induced heating intensity I when the sea surface temperature (SST) is 28.5°C and the moisture decays upward exponentially with a water vapor scale height of 2.2 km (Wang 1988). Observations also show that the moisture perturbation has a comparable nondimensional magnitude with that of the temperature perturbation for the 2-day waves (Takayabu et al. 1996; Haertel and Kiladis 2004). For example, the temperature and moisture perturbation amplitude is 0.3 K and 0.4 g kg^{-1} in the lower troposphere, respectively (Haertel and Kiladis 2004), and nondimensional amplitude is 0.12 and 0.18 according to the characteristic values listed in Table 1, respectively. The moisture anomalies are stronger than the temperature anomalies. For simplicity, we introduce a parameter a_q to represent this nondimensional ratio, and represent

$$\tilde{M} = a_q + (1 - a_q)H_j. \qquad (24)$$

Substituting Eqs. (23) and (24) into Eqs. (13) and (14), we can find that the moisture perturbation amplitude is

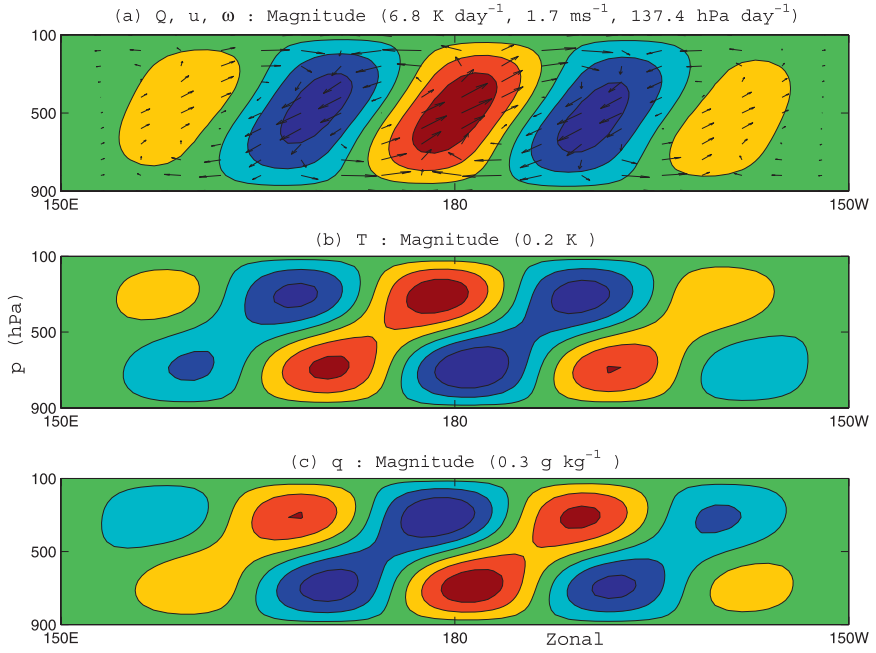

FIG. 3. Velocity vectors and contours of synoptic-scale (a) heating (red) and cooling (blue), (b) temperature, and (c) moisture perturbations above the equator as functions of zonal and pressure coordinates for the eastward-tilted 2-day waves. Contour interval is one-third of the perturbation amplitude. The contours and vectors are scaled to their respective maximum magnitudes: (a) 6.8 K day^{-1}, 1.7 m s^{-1}, and 137.4 hPa day^{-1}; (b) 0.2 K; and (c) 0.3 g kg^{-1}. Here $a_q = 1.5$.

a_q times the temperature perturbation amplitude. From Eq. (24), $\tilde{M}$ is proportional to a_q, which means that the moisture disturbance would increase with the increasing background moisture gradient.

So the solution of 2-day waves can be obtained for the forcing (22):

$$\begin{Bmatrix} u \\ v \\ \phi \end{Bmatrix} = -F(X) \sum_{j=1,2+,2-} \begin{Bmatrix} Mu_j \sin(kx - \sigma t + \phi_j) \\ Mv_j \cos(kx - \sigma t + \phi_j) \\ M\phi_j \sin(kx - \sigma t + \phi_j) \end{Bmatrix} \times \cos(jp), \tag{25a}$$

$$\begin{Bmatrix} \omega \\ T \\ q \end{Bmatrix} = F(X) \sum_{j=1,2+,2-} \begin{Bmatrix} M\omega_j \cos(kx - \sigma t + \phi_j) \\ MT_j \sin(kx - \sigma t + \phi_j) \\ Mq_j \sin(kx - \sigma t + \phi_j) \end{Bmatrix} \times \sin(jp), \tag{25b}$$

where Eqs. (25) are derived in appendix A.

These solutions [Eqs. (25)] simulate the observed 2-day waves under the given heating structure. The pronounced backward tilt is well reproduced (Fig. 3a), and it is excited by the given heating source. The upward motion is usually in phase with the positive heating source. In this solution, not only the structures but also the amplitudes are in accord with the observations (Haertel and Kiladis 2004). For example, for the given heating amplitude of 6.8 K day^{-1}, the excited horizontal and vertical motions have amplitudes of 1.7 m s^{-1} and 137.4 hPa day^{-1}, respectively (Fig. 3a).

From Eqs. (25b) and (A8), the moisture perturbation is almost out of phase with the temperature perturbation (Figs. 3b,c), and this is consistent with the lower tropospheric observations (Takayabu et al. 1996; Haertel and Kiladis 2004). Since the moisture perturbation not only has the comparable amplitude (when $a_q = 1$), but also the out-of-phase structure with the temperature perturbation (Fig. 3c), the EQT becomes as important as the EMT and EHT. Different from the solution derived under the geostrophic approximation, which has an off-equatorial maximum temperature perturbation (Majda and Biello 2004), the disturbances under the ageostrophic approximation here are all trapped near the equator (Fig. 4). As such, our new solution for the 2-day waves may provide a strong EHT, which is not negligible compared with the momentum transfer. The simulated horizontal structures resemble those of the $n = 1$ westward inertio-gravity waves (Fig. 4). In the lower troposphere (850 hPa), the temperature perturbations are nearly in phase with the zonal winds and lead the wave convergence

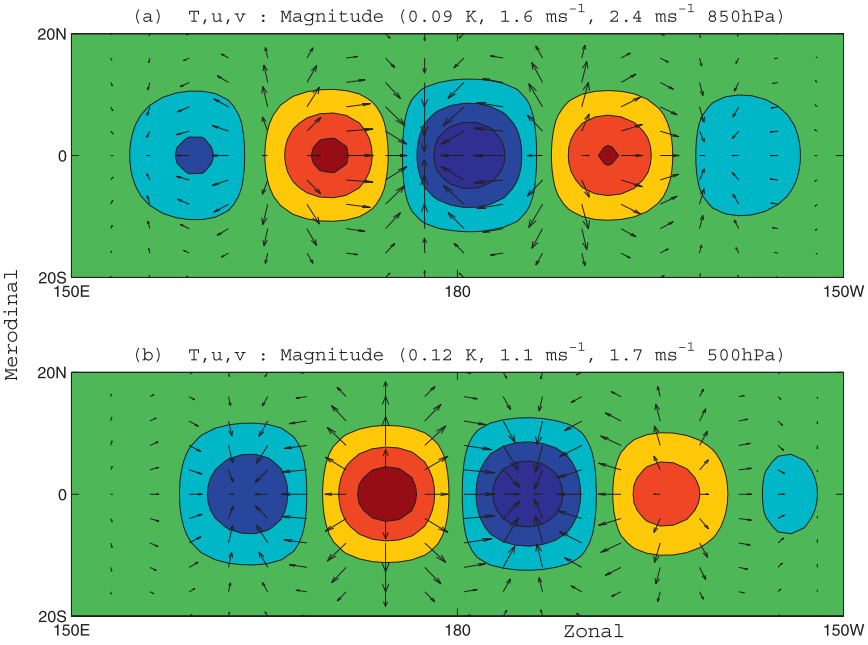

FIG. 4. Velocity vectors and contours of synoptic-scale positive (red) and negative (blue) temperature perturbations as functions of zonal and meridional coordinates at (a) 850 and (b) 500 hPa. Contour intervals are as in Fig. 1. The contours and vectors are scaled to their respective maximum magnitudes: (a) 0.09 K, 1.6 m s^{-1}, and 2.4 m s^{-1}; (b) 0.12 K, 1.1 m s^{-1}, and 1.7 m s^{-1}.

(Fig. 4a). The lower tropospheric disturbances (Fig. 4a) also lead the middle tropospheric disturbances (Fig. 4b), which produces a vertical tilted structure and allows nonzero upscale eddy flux transfers.

4. The EMT, EHT, and EQT associated with the 2-day waves

Based on the solution [Eqs. (25)], we can obtain explicit representations of the EMT, EHT, and EQT associated with the 2-day waves [i.e., Eqs. (B4)–(B6)]. Details of the derivation are reported in appendix B. The upscale eddy property transfer is drawn in Fig. 5. The EMT has the same structure as that provided by Majda and Biello (2004), but with an opposite phase (Fig. 5a). The eastward-tilted 2-day waves produce a lower tropospheric easterly and an upper tropospheric westerly EMT. Because the 2-day waves are trapped near the equator (Fig. 4), the EHT also has its maximum value at the equator (Fig. 5b), and its nondimensional amplitude is about 0.9 times of that of the EMT (Fig. 5b). The EHT tends to cool down the middle troposphere. In Fig. 5c, the EQT has the same structure as that of the EHT and also has comparable amplitude. Different from the negative EHT, the EQT is always positive in the middle troposphere, which means that the 2-day waves tend to moisten the middle troposphere on the planetary scale.

The first baroclinic mode can represent the deep convection of the moist Kelvin waves very well (Wang 1988), which provides an easy way to understand the interaction in the moist Kelvin waves. To study this interaction, we try to establish a simple baroclinic SI model, where the eddy flux envelope of the 2-day waves can be easily represented by the large-scale motions. So we take a look at the first baroclinic EMT, EHT, and EQT, which can be written as

$$F^U = \kappa_U \cos(p), \tag{26}$$

$$F^T = -\kappa_T \sin(p), \tag{27}$$

$$F^q = -a_q F^T. \tag{28}$$

Details of derivation for Eqs. (26)–(28) are presented in appendix B. For the first baroclinic mode, the EMT produces lower tropospheric easterly and upper tropospheric westerly (Fig. 6a), and the EHT cools down the middle troposphere (Fig. 6b). Meanwhile the EQT tends to moisten the middle troposphere (Fig. 6c). The nondimensional amplitude of EHT or EQT accounts for about half of that of EMT when $a_q = 1$.

In previous works, the use of geostrophic approximation for the synoptic-scale motions yielded a very weak EHT (Majda and Biello 2004; Biello and Majda 2005;

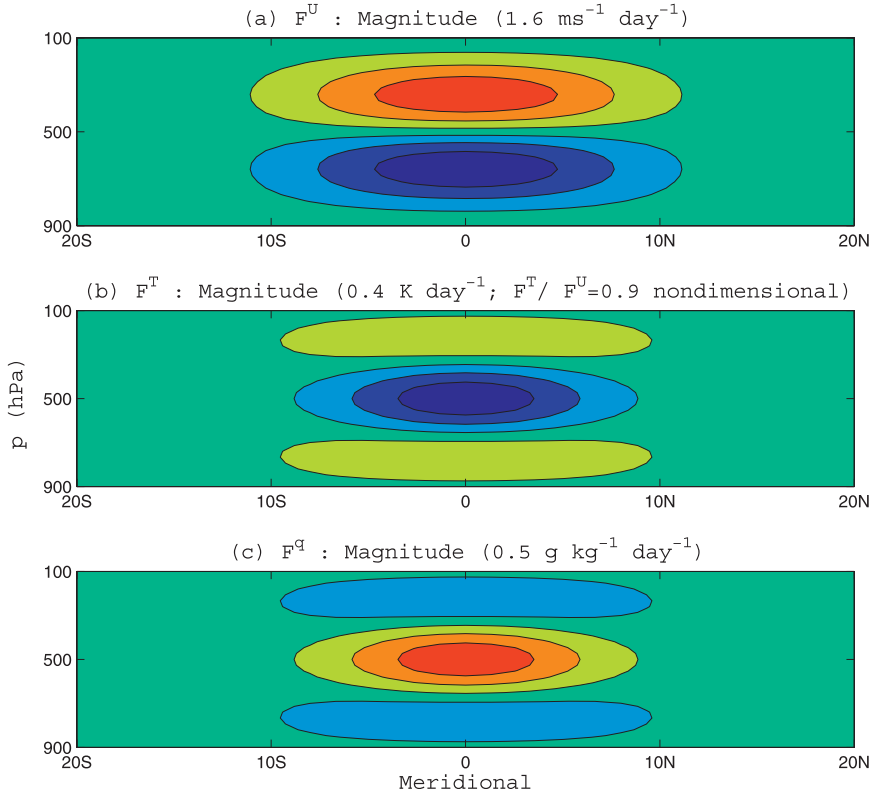

FIG. 5. Contours of (a) westerly (red) and easterly (blue) EMT, (b) positive (red) and negative (blue) EHT, and (c) positive (red) and negative (blue) EQT. Contour intervals are as in Fig. 1. The contours are scaled to their respective maximum magnitudes: (a) 1.6 m s^{-1} day^{-1}, (b) 0.4 K day^{-1}, and (c) 0.5 g kg^{-1} day^{-1}. The nondimensional amplitude ratio of the EHT to the EMT is 0.9. Here $a_q = 1.5$.

Wang and Liu 2011), and the role of EHT was neglected. Like the EMT that can provide an instability source for the MJO (Wang and Liu 2011), our results here show that the strong EHT of the 2-day waves may also provide an instability source or sink for the planetary-scale motions.

5. The moist Kelvin waves interacting with the 2-day waves

a. First baroclinic SI model

There is an easy way to discuss the first baroclinic interaction between the moist Kelvin waves and the 2-day waves. For the moist Kelvin waves, we neglect the temporal variation of the moisture perturbation [i.e., $\overline{q}_t = 0$ in Eq. (20)] (Wang 1988). The truncated first baroclinic SI model can be obtained by substituting Eqs. (26)–(28) into Eqs. (15)–(20):

$$\overline{U}_{t_L} = -\overline{\Phi}_X - \kappa_U, \tag{29}$$

$$y\overline{U} = -\overline{\Phi}_y, \tag{30}$$

$$\overline{U}_X - \overline{\Omega} = 0, \tag{31}$$

$$\overline{\Phi}_{t_L} + \overline{\Omega} = -\overline{Q} + \kappa_T, \tag{32}$$

$$\overline{\tilde{M}}\,\overline{\Omega} = -\overline{Q} + a_q\kappa_T, \tag{33}$$

where the two interaction parameters κ_U and κ_T represent the envelope of the EMT and EHT, respectively, and the EQT amplitude is a_q times the EHT amplitude. To build a real two-way SI model, we have to find the relationship between the eddy flux envelope and the large-scale motions. In the one-way SI model, the role of the synoptic-scale motions on the large-scale motions can be studied with κ_U and κ_T given (Majda and Biello 2004; Biello and Majda 2005), while the growth rate and phase speed cannot be studied by these one-way SI models.

b. Observations

1) When the moist Kelvin waves meet with the 2-day waves, observations show that the 2-day waves are

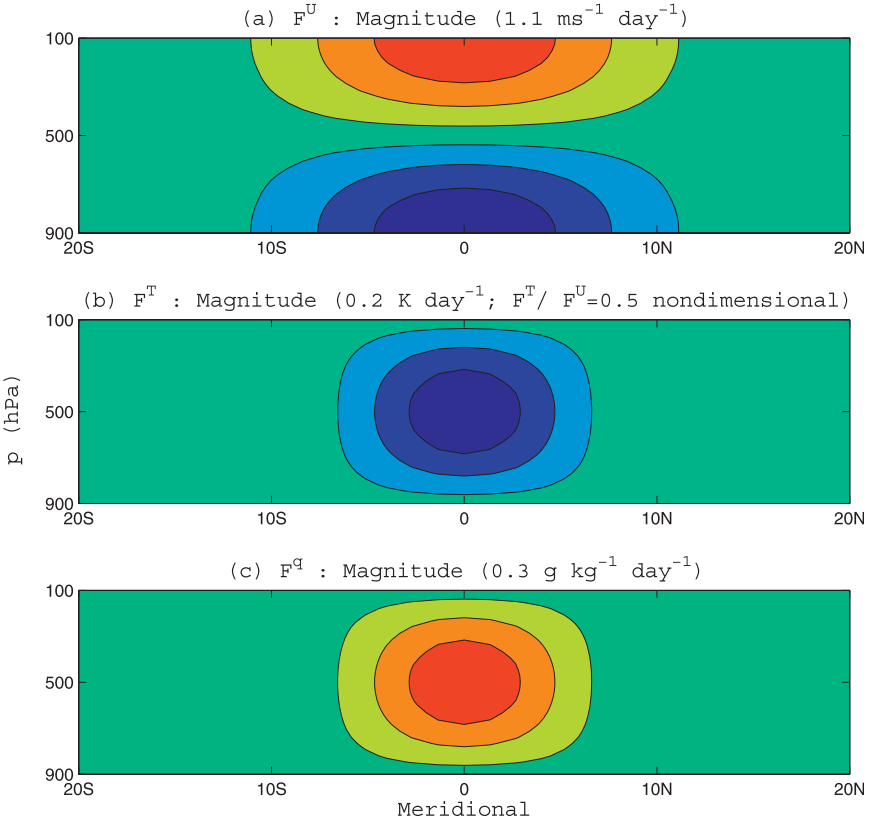

FIG. 6. As in Fig. 5, but for the first baroclinic mode. The contours are scaled to their respective maximum magnitudes: (a) 1.1 m s^{-1} day^{-1}, (b) 0.2 K day^{-1}, and (c) 0.3 g kg^{-1} day^{-1}. The nondimensional amplitude ratio of the EHT to the EMT is 0.5.

more enhanced near the convective complex of the moist Kelvin waves (Fig. 1).

2) The 2-day waves also show asymmetric phase relationship with the large-scale motions, and they are more active to the east of the moist Kelvin wave or the MJO that has a Kelvin wave component (Fig. 1). As a "self-similarity" system, the moist Kelvin wave excites the Ekman pumping under its low-pressure region (Wang 1988), where the lower tropospheric moisture is plenteous and provides enough energy for the growth of the 2-day waves. After the strong convection associated with the passing Kelvin waves, the 2-day waves begin to decay in the region where the stratiform clouds prevail.
3) The enhanced activity of the 2-day waves tends to coincide with, or shift a little bit to the east of, the short Kelvin waves, which tends to occur to the east of the MJO that has a long Kelvin wave component (Fig. 1). This implies a dependence of phase lag on wavelength.

c. *Parameterization of the eddy flux envelope*

Based on observation 1 that the 2-day waves are controlled by the large-scale convective complex, we assume that the eddy flux envelope is proportional to the large-scale diabatic heating $\overline{Q}$ or the large-scale vertical pressure velocity $\overline{\Omega}$. By this assumption the strength of the 2-day waves is proportional to $\sqrt{\overline{\Omega}}$. Furthermore, based on observation 2 that the 2-day waves are more enhanced to the east of the moist Kelvin waves or the MJO that has a Kelvin wave component, we assume that the eddy flux envelope of the 2-day waves leads (in the direction of eastward propagation) the convection center of the moist Kelvin wave by a phase $\overline{\phi}$. Based on these two assumptions, the eddy flux envelopes can be parameterized as

$$\kappa_U = C_U R_e(-\overline{\Omega} e^{-i\overline{\phi}}), \tag{34}$$

$$\kappa_T = C_T R_e(-\overline{\Omega} e^{-i\overline{\phi}}), \tag{35}$$

where C_U and C_T are two positive SI coefficients associated with the EMT and EHT, respectively.

It is necessary to determine these two SI coefficients to complete the SI model. The moisture Eq. (33) presents $\overline{Q} \approx -\tilde{M}\overline{\Omega}$ and the EHT Eq. (35) obeys $\kappa_T = -C_T\overline{\Omega}\cos(\overline{\phi})$. After dividing the latter by the former we

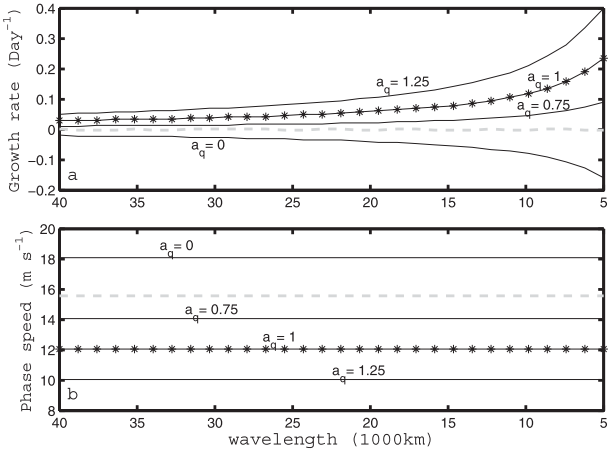

FIG. 7. (a) Growth rate and (b) phase speed as a function of wavelength for the SI of moist Kelvin waves. The amplitude ratio of EQT to EHT a_q is 0, 0.75, 1, and 1.25, respectively. Here $\overline{\phi} = \pi/4$. The dashed lines represent the free moist Kelvin waves, and the starred lines represent the SI moist Kelvin waves only interacting with EMT.

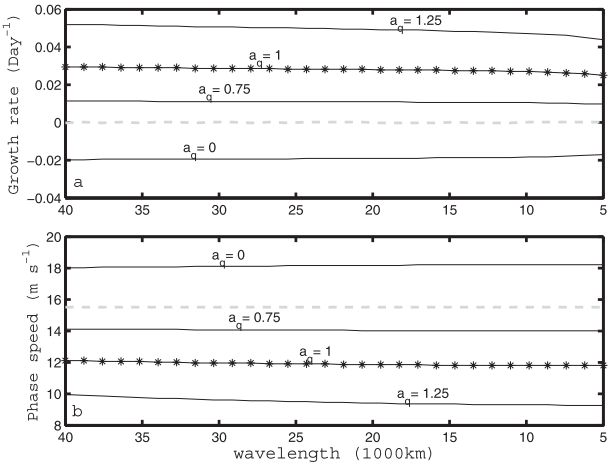

FIG. 8. As in Fig. 7, but $\overline{\phi}$ depends on the wavelength and is determined by Eq. (38).

can obtain $C_T \approx (\kappa_T/\overline{Q})[\overline{\tilde{M}}/\cos(\overline{\phi})]$. The nondimensional mean vertical moisture gradient $\tilde{M}$ is taken as 0.9, the standard value for the low-frequency motions (Yano and Emanuel 1991; Frierson et al. 2004; Majda and Stechmann 2009, 2011). Compared with the observations (Lin and Johnson 1996; Yanai et al. 2000), the diabatic heating amplitudes, $Q \approx 6.8$ K day^{-1} and $\overline{Q} \approx 1.5$ K day^{-1}, are good estimates for the synoptic- and planetary-scale heating rates, respectively. Our results also show that the 2-day waves with magnitude of 6.8 K day^{-1} (Fig. 3a) can produce a negative EHT with magnitude of 0.2 K day^{-1} ($F^T = -\kappa_T \approx -0.2$ K day^{-1}) on the planetary scale (Fig. 6b). When $\overline{\phi} = \pi/4$ we can calculate that $C_T \approx 0.15$.

For the simulated 2-day waves, the EMT and EHT have the similar meridional structures to the lowest order, and the EMT amplitude is about twice the EHT amplitude (Fig. 6), so the EMT and EHT are parameterized to have the same horizontal envelopes with different amplitudes (i.e., $\kappa_U = \kappa_T/0.5$). Dividing Eq. (34) by Eq. (35), we obtain $C_U = C_T/0.5 \approx 0.3$.

d. Eigenvalue solutions

Assume that the wave structure has the form of

$$\{\overline{U}, \overline{\Phi}, \overline{T}, \overline{\Omega}\} = \{\overline{U}_0, \overline{\Phi}_0, \overline{T}_0, \overline{\Omega}_0\} e^{i(KX - \Gamma t_L)}, \quad (36)$$

where K and Γ are the large-scale wavenumber and frequency, respectively, and $\Gamma = \Gamma_r + i\Gamma_i$.

Substituting Eq. (36) into the SI model [Eqs. (29)–(33)], we can obtain the frequency equation for the SI moist Kelvin waves:

$$\Gamma^2 + [\cos(\overline{\phi})C_U K - i\sin(\overline{\phi})C_U K]\Gamma - [1 - \overline{\tilde{M}} - (1 - a_q)\cos(\overline{\phi})C_T]K^2 - i(1 - a_q)\sin(\overline{\phi})C_T K^2 = 0. \quad (37)$$

The growth rate $G_r = \mathrm{Im}(\Gamma)$ and phase speed $P_s = \mathrm{Re}(\Gamma/K)$ of the SI moist Kelvin waves are shown in Fig. 7 for $\overline{\phi} = \pi/4$. The moist Kelvin waves without interaction with the 2-day waves (dashed lines in Figs. 7–9) remain stable (dashed line in Fig. 7a), because the mean state troposphere is stable to wave convergence–induced instability (Wang 1988). Such free moist Kelvin waves propagate eastward fast (dashed line in Fig. 7b).

Figure 7 shows how the 2-day waves affect the moist Kelvin waves through the EMT, EHT, and EQT. The

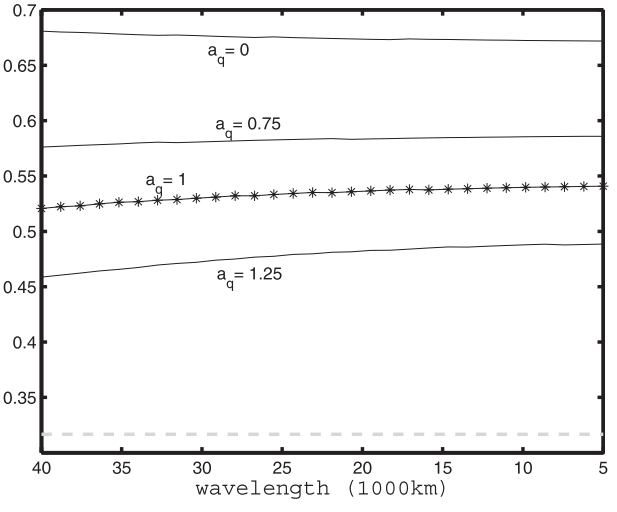

FIG. 9. Nondimensional e-folding scales as a function of wavelength. The e-folding scales are scaled to the Rossby radius of deformation. Here $\overline{\phi}$ is determined by Eq. (38).

EMT provides an instability source for the moist Kelvin waves, especially on the short scales (starred line in Fig. 7a). This upscale transfer-induced instability mainly comes from the projection of lower tropospheric easterly EMT on the lower tropospheric easterly of the moist Kelvin waves. The easterly EMT enhances the in-phase easterly of the moist Kelvin waves, but damps the out-of-phase westerly of the moist Kelvin waves. The negative EHT cools down the middle troposphere so as to damp the moist Kelvin waves, and it even overwhelms the positive role of EMT. This negative role is also on the short scales (line $a_q = 0$ in Fig. 7a).

The EQT provides another instability source for the moist Kelvin waves (lines $a_q > 0$ in Fig. 7a). In this SI model, the 2-day waves transfer the boundary layer moisture into the middle troposphere and enhance the deep convection associated with the moist Kelvin waves through the upscale EQT. For the observational 2-day waves, a_q is usually greater than 1 (Takayabu et al. 1996; Haertel and Kiladis 2004), and the positive role of EQT overwhelms the negative effect of the EHT (line $a_q =$ 1.25 in Fig. 7a), and the 2-day waves yield larger instabilities for the moist Kelvin waves. The unstable moist Kelvin waves suffer a short wave blow-up in the absence of the heating due to the planetary boundary layer–induced moisture convergence (Wang 1988).

The 2-day waves also affect the phase speed of the moist Kelvin waves (Fig. 7b). The EMT tends to slow down the moist Kelvin waves (starred line in Fig. 7b). The cause is the advective effect of the lower tropospheric easterly EMT. Substituting the EMT Eq. (34) and the continuity Eq. (31) into the planetary-scale momentum Eq. (29) yields an effective planetary-scale equation $U_{t_L} - C_U \cos(\overline{\phi}) U_X = -\Phi_X$, in which the EMT acts as a Dropper shift. The EHT accelerates the moist Kelvin waves (line $a_q = 0$ in Fig. 7b) because it cools down the middle troposphere and reduces the convective available potential energy in the front of the moist Kelvin waves (Lin and Johnson 1996; Wang and Xie 1998). The EQT moistens the middle troposphere and enhances the slowly propagating moist Kelvin waves (line $a_q = 1.25$ in Fig. 7b).

e. Wavelength-dependent phase lag

Based on observation 3 that enhanced activity of the 2-day waves tends to coincide with, or shift a little bit to the east of, the short Kelvin waves, which tends to occur to the east of the MJO that has a long Kelvin wave component, we assume that the phase lag $\overline{\phi}$ depends weakly on the wavelength:

$$\overline{\phi} = \frac{L - L_S}{L_L - L_S}(\overline{\phi}_L - \overline{\phi}_S) + \overline{\phi}_S, \tag{38}$$

TABLE 2. Nondimensional SI parameters used in the model.

Physical quantity	Name	Value or unit scale
EHT coefficient	C_T	~0.15
EMT coefficient	C_U	~0.3
Amplitude ratio of EQT to EHT	a_q	~1
Phase lag between deep convection and congestus/stratiform in the 2-day waves	ϕ_0	$\pi/4$
Longest wavelength of moist Kelvin waves	L_L	5.3 (40 000 km)
Shortest wavelength of moist Kelvin waves	L_S	0.7 (5000 km)
Maximum phase between 2-day and Kelvin waves	$\overline{\phi}_L$	$\pi/4$
Minimum phase between 2-day and Kelvin waves	$\overline{\phi}_S$	$\pi/36$

where L is the wavelength of the moist Kelvin waves, L_L is the longest wavelength (40 000 km), and L_S is the shortest wavelength (5000 km). Note that $\overline{\phi} = \overline{\phi}_L$ if $L = L_L$, while $\overline{\phi} = \overline{\phi}_S$ when $L = L_S$. These SI parameters are listed in Table 2.

The results of this model are shown in Fig. 8. Although they are similar to the results in Fig. 7, there are notable differences. The EMT and EQT both provide instability sources for the moist Kelvin waves, while the EHT damps these moist Kelvin waves (Fig. 8a). The 2-day waves also slow down the moist Kelvin waves (Fig. 8b). Determined by this wavelength-dependent phase lag $\overline{\phi}$, this SI model no longer suffers the short wave blow-up problem (Fig. 8a), and the long moist Kelvin waves become more unstable. This wave selection is parameter dependent, and it becomes more obvious when $\overline{\phi}_S = 0$—that is, when the eddy flux envelope of the 2-day waves coincides with the shortest moist Kelvin wave center. The growth rate decays rapidly at short waves (not shown), and the results show that the wavelength-dependent phase lag is important for the moist Kelvin waves to become unstable at long wavelengths. Of course, this is a crucial assumption based on observation 3, and further observations are needed to study this wavelength-dependent scale interaction.

f. Horizontal structures

The horizontal structure of the SI moist Kelvin waves can be obtained from Eqs. (29)–(33) and (35)

$$\Phi = R_e\left(\Phi_0 \exp\left\{\Gamma_i t_L - \frac{y^2}{2L_y^2} + i\left[KX + \frac{y^2}{2L_y^2}\frac{\Gamma_i - \sin(\overline{\phi})KC_u}{\Gamma_r + \cos(\overline{\phi})KC_u} - \Gamma_r t_L\right]\right\}\right), \tag{39}$$

where the *e*-folding scale of the meridional extent of these moist Kelvin waves is represented as

$$L_y = \sqrt{\frac{[\Gamma_r + \cos(\overline{\phi})KC_u]^2 + [\Gamma_i - \sin(\overline{\phi})KC_u]^2}{K[\Gamma_r + \cos(\overline{\phi})KC_u]}}. \quad (40)$$

The EMT extends the meridional extent of these moist Kelvin waves (starred line in Fig. 9). The EHT tends to increase the *e*-folding scale (line $a_q = 0$ in Fig. 9), while the EQT tends to decrease it. When interacting with the 2-day waves, the unstable moist Kelvin waves have a broader meridional scale than the free moist Kelvin waves, and the major reason is the effect of the EMT.

Equation (39) also reveals that the moist Kelvin waves have a meridional phase propagation associated with the eastward propagation. The meridional phase speed can be written as

$$\frac{y}{t_L} = \frac{2\Gamma_r L_y^2}{y}\frac{\Gamma_r + \cos(\overline{\phi})KC_u}{\Gamma_i - \sin(\overline{\phi})KC_u}. \quad (41)$$

As in the results of Wang (1988), the meridional phase speed decreases with increasing latitude. The results also suggest that the EMT could force the unstable moist Kelvin waves to propagate equatorward, while the unstable moist Kelvin waves without the EMT usually propagate poleward (not shown).

6. Summary and discussion

a. Impact of ageostrophic approximation on the 2-day wave dynamics

Our analytical solution simulates both the structure and amplitude of the 2-day waves, as it captures the essence of the 2-day waves, which is the coupling of the ageostrophic $n = 1$ inertio-gravity waves with the congestus, deep convective, and stratiform heating. This solution not only produces a lower tropospheric easterly eddy momentum transfer (EMT) that is in accord with the previous works (Biello and Majda 2005) but also produces an equatorial trapped negative eddy heating transfer (EHT) that has an amplitude comparable to that of the EMT. The geostrophic approximation produces a reasonable EMT of the 2-day waves (Biello and Majda 2005), but it misrepresents the temperature perturbation, which has an off-equatorial maximum value and produces a negligibly small EHT.

Our results show that the EHT for the convectively coupled Kelvin waves is also different from that obtained by Biello and Majda (2005): The EHT for the convectively coupled Kelvin waves is equatorially trapped and has comparable amplitude with that of the EMT.

b. The strong eddy moisture transfer effect

The new analytical solution presented in this work shows strong moisture perturbation with a period of 2 days, in accord with observations (Takayabu et al. 1996; Haertel and Kiladis 2004). The moisture perturbation is nearly out of phase with the temperature perturbation, but has comparable amplitude. So this solution of the 2-day waves gives an equatorial trapped eddy moisture transfer (EQT), which tends to moisten the middle troposphere.

c. The instability sources and the reasons for reduced propagation speed

In the scale-interaction (SI) model, the 2-day waves not only slow down the moist Kelvin waves through the advective effect of the EMT, but also provide an instability source through both the EMT and the EQT. Although the EHT damps the moist Kelvin waves, the positive role of EQT usually overwhelms its negative role for the observed 2-day waves.

d. Explaining the convective enhancement

In observations, the low-frequency moist Kelvin waves, as well as the MJO, experience convective enhancement when meeting with the 2-day waves (Figs. 1 and 2). Our model results suggest that the 2-day waves can provide an instability source for the moist Kelvin waves and slow down their movement (Figs. 7 and 8). To support this claim, we made a composed diagram based on the model results. For the moist Kelvin waves with wavelength of 25 000 km, their instability envelope $I(t_L)$ along the equator is defined as

$$I(t_L) = G_r(t_L)\exp\left\{-\left[\frac{X - X_0 - P_s(t_L)t_L}{L_M}\right]^2\right\}, \quad (42)$$

where the growth rate $G_r(t_L)$ and the phase speed $P_s(t_L)$ are related to a time series of eddy flux amplitude $C_T(t_L)$ of the 2-day waves. The amplitude and speed of the instability envelope are determined by the growth rate and phase speed calculated from Eq. (37). The initial center location $X_0 = 100°$E, and the length scale of the envelope $L_M = 10°$. A time–longitude evolution of $C_T(t_L)$ is given in Fig. 10 with one strong and two weak peaks of C_T appearing near days 3, 1.3, and 4.7, respectively, when the 2-day wave envelopes are strong. All parameters are listed in Tables 1 and 2, except for $a_q = 1.25$.

In Fig. 10, as propagating eastward, the moist Kelvin waves exhibit three growth rate centers when meeting

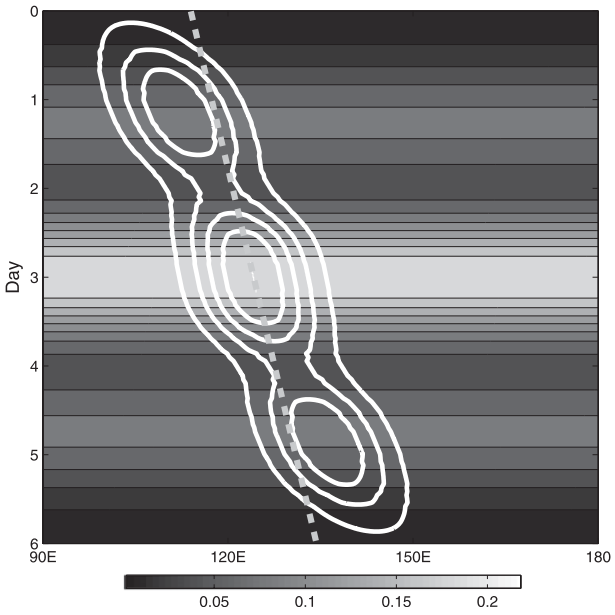

FIG. 10. Hovmöller diagram of the instability envelope (contours) of the SI moist Kelvin wave with wavelength of 25 000 km. The C_T evolution is shaded. The reference phase speed line of 5 m s^{-1} is shown by the dashed line. The maximum instability is 0.1 day^{-1}, and contour interval is 0.02 day^{-1}.

with the 2-day waves, suggesting that the moist Kelvin waves grow fast there and show convective enhancement. The strong moist Kelvin waves are slowed down heavily when meeting with the enhanced 2-day waves at day 3. This result may also help understand the convective enhancement of the MJO, which has a strong Kelvin wave component (Wang and Rui 1990).

e. Limitation of this work

The theoretical results presented here explain why the low-frequency moist Kelvin waves or the MJO exhibit convective enhancement when meeting with the high-frequency 2-day waves, although only the first baroclinic mode was included in this SI model. In the future work, the second baroclinic mode associated with the congestus and stratiform clouds of moist Kelvin waves and MJO (Khouider and Majda 2006, 2007; Waite and Khouider 2009) will be included in this SI model. Especially, the boundary layer processes should be implemented into this SI model, which may improve the idealized phase function [Eq. (38)] between the 2-day wave envelope and the moist Kelvin wave convective center. Meanwhile, the convective downdraft of the 2-day waves is important when considering the high-order baroclinic modes (Haertel and Kiladis 2004).

The simple linear closure assumption is a weakness of this paper. The prediction model of the 2-day waves, such as the cloud-resolving model (Kuang 2008) or multicloud model (Khouider and Majda 2006, 2007), should be implemented into the SI model in the future work; then we can compare the linear and nonlinear processes in the SI.

Validation of these theoretical results requires high-resolution observations on the multiscale structures within the MJO and moist Kelvin waves with different wavelengths.

Acknowledgments. This study was supported by Climate Dynamics Program of the National Science Foundation under Award AGS-1005599 and Global Research Laboratory (GRL) Program from the Ministry of Education, Science, and Technology (MEST), Korea. Additional support was provided by the Japan Agency for Marine-Earth Science and Technology (JAMSTEC), by NASA through Grant NNX07AG53G, and by NOAA through Grant NA17RJ1230 through their sponsorship of research activities at the International Pacific Research Center.

APPENDIX A

The Solution for the 2-Day Waves

Substituting Eq. (23) into Eqs. (13)–(14), Eqs. (9)–(14) can be written on the jth baroclinic mode:

$$u_{jt} - yv_j = -\phi_{jx}, \tag{A1}$$

$$v_{jt} + yu_j = -\phi_{jy}, \tag{A2}$$

$$T_j = -j\phi_j, \tag{A3}$$

$$u_{jx} + v_{jy} - j\omega_j = 0, \tag{A4}$$

$$T_{jt} - \omega_j = -H_j\omega_j, \tag{A5}$$

$$q_{jt} + \tilde{M}\omega_j = H_j\omega_j. \tag{A6}$$

The analytical solution for the jth mode can be obtained according to the work of Matsuno (1966), and the idea of the reduced stability is applied to both the first and second baroclinic modes. Assuming that different vertical modes of the 2-day waves have the same structure of $e^{i(kx-\sigma t)}$, $k = -3.5$ (with wavelength of 2500 km) and $\sigma = 1.1$ (with period of 2 days) are the wavenumber and frequency, respectively. Then the solution for the jth mode can be written as

$$\{u_j, v_j, \omega_j, T_j, q_j, \phi_j\} = \{Mu_j \sin(kx - \sigma t),\ Mv_j \cos(kx - \sigma t),\ M\omega_j \cos(kx - \sigma t),\ MT_j \sin(kx - \sigma t),\ Mq_j \sin(kx - \sigma t),\ M\phi_j \sin(kx - \sigma t)\}, \tag{A7}$$

where

$$\{Mu_j, Mv_j, M\omega_j, MT_j, Mq_j, M\phi_j\} = \{jQ_jC_r(r_1D_2 - r_2D_0)/2,\ jQ_jC_rD_1,\ Q_j\sigma(r_1D_2 + r_2D_0)/2,\ -j^2Q_jC_r^2(r_1D_2 + r_2D_0)/2,\ -a_qMT_j,\ jQ_jC_r^2(r_1D_2 + r_2D_0)/2\} \tag{A8}$$

and

$$\{r_1, r_2\} = \{\sqrt{C_r}/(kC_r - \sigma), \sqrt{C_r}(kC_r + \sigma)\}. \tag{A9}$$

The phase speed C_r is the same for both the first and second baroclinic modes, and it is determined by the frequency equation of the $n = 1$ westward inertio-gravity waves,

$$\sigma^2/C_r^2 = k^2 + 3/C_r, \tag{A10}$$

where $C_r = 0.23$ (dimensional value: 14.5 m s^{-1}), and the positive constant H_j is determined as

$$H_j = 1 - j^2C_r^2, \tag{A11}$$

where $H_1 = 0.95$ and $H_2 = 0.8$.

The meridional structure of waves is given in terms of parabolic cylinder functions D, which takes the form

$$D_s = \exp[-(y/2\sqrt{C_r})^2]P_s(y/\sqrt{C_r}), \tag{A12}$$

where P_s is a polynomial of degree s.

APPENDIX B

The EMT, EHT, and EQT Associated with the 2-Day Waves

The EMT, EHT, and EQT are defined as

$$F^U = -\overline{(uv)}_y - \overline{(u\omega)}_p, \tag{B1}$$

$$F^T = -\overline{(Tv)}_y - \overline{(T\omega)}_p, \tag{B2}$$

$$F^q = -\overline{(qv)}_y - \overline{(q\omega)}_p. \tag{B3}$$

Substituting Eq. (25) into Eqs. (B1)–(B3), the upscale eddy property transfer can be written explicitly as

$$F^U = \frac{3C_r}{16}\frac{Q_1Q_{2+} - Q_1Q_{2-}}{H_1H_2}\sigma(r_1D_2^2 - r_2D_0^2)\sin(\phi_0) \times [-\cos(3p) + \cos(p)], \tag{B4}$$

$$F^T = -\frac{C_r^3}{4}\frac{Q_1Q_{2+} - Q_1Q_{2-}}{H_1H_2}(r_1D_2D_1 + r_2D_0D_1)_y \sin(\phi_0) \times [(\sin(3p) + 3\sin(p)] + \frac{3C_r^2}{16}\frac{Q_1Q_{2+} - Q_1Q_{2-}}{H_1H_2} \times \sigma(r_2D_2 + r_2D_0)^2 \sin(\phi_0)[-3\sin(3p) + \sin(p)], \tag{B5}$$

$$F^q = -a_qF^T. \tag{B6}$$

To simplify the study of the SI in the moist Kelvin waves, only the first baroclinic mode is included in the first step. So the upscale eddy property transfer on the first baroclinic mode can be obtained from Eqs. (B4)–(B6):

$$F^U = \kappa_U \cos(p), \tag{B7}$$

$$F^T = -\kappa_T \sin(p), \tag{B8}$$

$$F^q = -a_qF^T, \tag{B9}$$

where the two positive parameters κ_U and κ_T are

$$\kappa_U = \frac{3C_r}{16}\frac{Q_1Q_{2+} - Q_1Q_{2-}}{H_1H_2}\sigma(r_1D_2^2 - r_2D_0^2)\sin(\phi_0), \tag{B10}$$

$$\kappa_T = -\frac{3C_r^3}{4}\frac{Q_1Q_{2+} - Q_1Q_{2-}}{H_1H_2}(r_1D_2D_1 + r_2D_0D_1)_y \sin(\phi_0) + \frac{3C_r^2}{16}\frac{Q_1Q_{2+} - Q_1Q_{2-}}{H_1H_2}\sigma(r_1D_2 + r_2D_0)^2 \sin(\phi_0). \tag{B11}$$

REFERENCES

Biello, J. A., and A. J. Majda, 2005: A new multiscale model for the Madden–Julian oscillation. *J. Atmos. Sci.,* **62,** 1694–1721.

Frierson, D., A. J. Majda, and O. Pauluis, 2004: Large-scale dynamics of precipitation fronts in the tropical atmosphere: A novel relaxation limit. *Comm. Math. Sci.,* **2,** 591–626.

Haertel, P. T., and G. N. Kiladis, 2004: Dynamics of 2-day equatorial waves. *J. Atmos. Sci.,* **61,** 2707–2721.

——, ——, A. Denno, and T. Rickenbach, 2008: Vertical mode decompositions of 2-day waves and the Madden–Julian oscillation. *J. Atmos. Sci.,* **65,** 813–833.

Johnson, R. H., T. M. Rickenbach, S. A. Rutledge, P. E. Ciesielski, and W. H. Schubert, 1999: Trimodal characteristics of tropical convection. *J. Climate,* **12,** 2397–2418.

Khouider, B., and A. J. Majda, 2006: A simple multicloud parameterization for convectively coupled tropical waves. Part I: Linear analysis. *J. Atmos. Sci.,* **63,** 1308–1323.

——, and ——, 2007: A simple multicloud parameterization for convectively coupled tropical waves. Part II. Nonlinear simulations. *J. Atmos. Sci.,* **64,** 381–400.

Kikuchi, K., and B. Wang, 2010: Spatiotemporal wavelet transform and the multiscale behavior of the Madden–Julian oscillation. *J. Climate,* **23,** 3814–3834.

Kiladis, G. N., M. C. Wheeler, P. T. Haertel, K. H. Straub, and P. E. Roundy, 2009: Convectively coupled equatorial waves. *Rev. Geophys.,* **47,** RG2003, doi:10.1029/2008RG000266.

Kuang, Z., 2008: A moisture-stratiform instability for convectively coupled waves. *J. Atmos. Sci.,* **65,** 834–854.

Lin, X., and R. H. Johnson, 1996: Kinematic and thermodynamic characteristics of the flow over the western Pacific warm pool during TOGA COARE. *J. Atmos. Sci.,* **53,** 695–715.

Madden, R., and P. Julian, 1971: Detection of a 40-50 day oscillation in the zonal wind in the tropical Pacific. *J. Atmos. Sci.,* **28,** 702–708.

——, and ——, 1994: Observations of the 40-50-day tropical oscillation—A review. *Mon. Wea. Rev.,* **122,** 814–837.

Majda, A. J., and R. Klein, 2003: Systematic multiscale models for the tropics. *J. Atmos. Sci.,* **60,** 393–408.

——, and J. A. Biello, 2004: A multiscale model for tropical intraseasonal oscillations. *Proc. Natl. Acad. Sci. USA,* **101,** 4736–4741.

——, and S. N. Stechmann, 2009: The skeleton of tropical intraseasonal oscillations. *Proc. Natl. Acad. Sci. USA,* **106,** 8417–8422.

——, and ——, 2011: Nonlinear dynamics and regional variations in the MJO skeleton. *J. Atmos. Sci.,* **68,** 2725–2743.

Maloney, E. D., and D. L. Hartmann, 1998: Frictional moisture convergence in a composite life cycle of the Madden–Julian oscillation. *J. Climate,* **11,** 2387–2403.

Mapes, B. E., 2000: Convective inhibition, subgrid-scale triggering energy, and ''stratiform instability'' in a toy tropical wave model. *J. Atmos. Sci.,* **57,** 1515–1535.

——, S. Tulich, J. Lin, and P. Zuidema, 2006: The mesoscale convection life cycle: Building block or prototype for large-scale tropical waves? *Dyn. Atmos. Oceans,* **42,** 3–29.

Matsuno, T., 1966: Quasi-geostrophic motions in the equatorial area. *J. Meteor. Soc. Japan,* **44,** 25–43.

Moncrieff, M. W., 2004: Analytic representation of the large-scale organization of tropical convection. *J. Atmos. Sci.,* **61,** 1521–1538.

Nakazawa, T., 1988: Tropical super clusters within intraseasonal variations over the western Pacific. *J. Meteor. Soc. Japan,* **66,** 823–836.

Takayabu, Y. N., 1994: Large-scale cloud disturbances associated with equatorial waves. Part II: Westward-propagating inertio-gravity waves. *J. Meteor. Soc. Japan,* **72,** 451–465.

——, K. M. Lau, and C. H. Sui, 1996: Observation of a quasi-2-day wave during TOGA COARE. *Mon. Wea. Rev.,* **124,** 1892–1913.

Tung, W.-W., and M. Yanai, 2002a: Convective momentum transport observed during the TOGA COARE IOP. Part I: General features. *J. Atmos. Sci.,* **59,** 1857–1871.

——, and ——, 2002b: Convective momentum transport observed during the TOGA COARE IOP. Part II: Case studies. *J. Atmos. Sci.,* **59,** 2535–2549.

Waite, M. L., and B. Khouider, 2009: Boundary layer dynamics in a simple model for convectively coupled gravity waves. *J. Atmos. Sci.,* **66,** 2780–2795.

Wang, B., 1988: Dynamics of tropical low-frequency waves: An analysis of the moist Kelvin wave. *J. Atmos. Sci.,* **45,** 2051–2065.

——, and H. Rui, 1990: Dynamics of the coupled moist Kelvin–Rossby wave on an equatorial β-plane. *J. Atmos. Sci.,* **47,** 397–413.

——, and X. Xie, 1998: Coupled modes of the warm pool climate system. Part I: The role of air–sea interaction in maintaining Madden–Julian oscillation. *J. Climate,* **11,** 2116–2135.

——, and F. Liu, 2011: A model for scale interaction in the Madden–Julian oscillation. *J. Atmos. Sci.,* **68,** 2524–2536.

Wheeler, M., and G. N. Kiladis, 1999: Convectively coupled equatorial waves: Analysis of clouds and temperature in the wavenumber–frequency domain. *J. Atmos. Sci.,* **56,** 374–399.

Yanai, M., B. Chen, and W.-W. Tung, 2000: The Madden–Julian oscillation observed during TOGA COARE IOP: Global view. *J. Atmos. Sci.,* **57,** 2374–2396.

Yano, J.-I., and K. A. Emanuel, 1991: An improved model of the equatorial troposphere and its coupling with the stratosphere. *J. Atmos. Sci.,* **48,** 377–389.